ADVANCED ENERGY MATERIALS
www.advenergymat.de

Field Effect Passivation in Perovskite Solar Cells by a LiF Interlayer

*Dorothee Menzel, Amran Al-Ashouri, Alvaro Tejada, Igal Levine, Jorge Andrés Guerra, Bernd Rech, Steve Albrecht, and Lars Korte**

The fullerene C_{60} is commonly applied as the electron transport layer in high-efficiency metal halide perovskite solar cells and has been found to limit their open circuit voltage. Through ultra-sensitive near-UV photoelectron spectroscopy in constant final state mode (CFSYS), with an unusually high probing depth of 5–10 nm, the perovskite/C_{60} interface energetics and defect formation is investigated. It is demonstrated how to consistently determine the energy level alignment by CFSYS and avoid misinterpretations by accounting for the measurement-induced surface photovoltage in photoactive layer stacks. The energetic offset between the perovskite valence band maximum and the C_{60} HOMO-edge is directly determined to be 0.55 eV. Furthermore, the voltage enhancement upon the incorporation of a LiF interlayer at the interface can be attributed to originate from a mild dipole effect and probably the presence of fixed charges, both reducing the hole concentration in the vicinity of the perovskite/C_{60} interface. This yields a field effect passivation, which overcompensates the observed enhanced defect density in the first monolayers of C_{60}.

1. Introduction

In the past decade, metal halide perovskites (MHP) have gained an enormous research interest as photoactive thin film absorbers, due to their versatile optoelectronic properties.[1] In only a few years, the power conversion efficiency (PCE) of single junction MHP solar cells has reached 25.5% in the n-i-p architecture.[2] Additionally, MHPs are ideal photoabsorbers for the top cell in tandem solar cell devices. When combined with a silicon bottom cell, they yield a record PCE of 29.8%,[3] already exceeding the physical limit for silicon single junction solar cells. For tandem solar cells, an "inverted", i.e. p-i-n layer stack is often preferred, as higher PCEs have been achieved due to lower parasitic absorption losses,[4,5] and their low-temperature processing enables a wider choice of bottom cells.

The device stability and PCE of silicon/perovskite tandem solar cells are crucially determined by the quality of the contact layer interfaces,[6,7] as they are found to limit especially the open circuit voltage (V_{OC}) and fill factor. Charge carrier selective contacts and their interfaces toward MHP absorbers are thus a field of recent and ongoing research.[8–10] The charge carrier transport across interfaces depends on two main parameters: The energy level alignment of both materials forming the interface, and the density of defect states at the surfaces and interfaces.

The fullerene C_{60} has become the standard electron transport layer (ETL) for p-i-n MHP solar cells. Similarly, it has also been applied in silicon/perovskite tandem solar cells with a p-i-n structure for the perovskite top cell, yielding the highest-efficiency devices in their class.[10] However, the obtained open circuit voltage for p-i-n MHP solar cells is found to be limited by the electron selective interface due to non-radiative recombination losses,[11,12] which raises interest in thoroughly studying the energetic formation of the perovskite/C_{60} interface, including the energy level alignment and density of gap states. The insertion of an ultra-thin (≈1 nm) LiF interlayer between the perovskite and C_{60} has been shown to significantly increase the device V_{OC} by reducing the non-radiative recombination while keeping a high

D. Menzel, A. Al-Ashouri, A. Tejada, I. Levine, S. Albrecht, L. Korte
Division Solar Energy
Helmholtz-Zentrum Berlin für Materialien und Energie GmbH
Hahn-Meitner-Platz 1, 14109 Berlin, Germany
E-mail: korte@helmholtz-berlin.de

A. Tejada, J. A. Guerra
Departamento de Ciencias
Sección Física
Pontificia Universidad Católica del Perú
Av. Universitaria 1801, Lima 15088, Peru

The ORCID identification number(s) for the author(s) of this article can be found under https://doi.org/10.1002/aenm.202201109.

DOI: 10.1002/aenm.202201109

I. Levine
Helmholtz-Zentrum Berlin für Materialien und Energie GmbH
Kekuléstraße 5, 12489 Berlin, Germany

B. Rech
Helmholtz-Zentrum Berlin für Materialien und Energie GmbH
Scientific Management
Hahn-Meitner-Platz 1, 14109 Berlin, Germany

B. Rech, S. Albrecht
Technical University Berlin
Faculty IV – Electrical Engineering and Computer Science
10587 Berlin, Germany

fill factor.[7,10,11] Several ideas are reported in the literature with LiF either chemically passivating defects in the perovskite or the C_{60}, creating a dipole, or even (partially) dissociating with the individual ions diffusing throughout the layer stack.[12–15] However, the exact mechanisms behind this are still poorly understood. Furthermore, since device stability deteriorates with the implementation of this LiF interlayer,[10] a better understanding of the underlying mechanisms can guide the search for other interlayers, which might yield similarly beneficial effects without sacrificing stability. In addition, it is of both academic and technological interest to unveil whether passivation mechanisms are comparable to the ones in established technologies, like, e.g., surface field passivation in silicon solar cells.[16]

Photoelectron spectroscopy (PES) is one of the most prominent and powerful experimental techniques to study the energy level alignment at semiconductor heterojunctions.[17,18] While most studies rely on ultraviolet He-I (21.2 eV) excitation (He-UPS),[19] near-UV photon excitation energies are less common.[20,21] Here, we apply UPS with 6.5 eV excitation energy (NUPS) and additionally vary the incident photon energy in the near-UV range from 3.7 to 7.3 eV and measure the excited photoelectrons per absorbed photon (yield) at one constant final state (fixed kinetic energy), hence the method is called constant final state yield spectroscopy (CFSYS).[22] It combines two main advantages: i) a very high signal-to-noise ratio can be achieved, 3–4 orders of magnitude higher than typical He-UPS. Together with a varying photon flux over the incident photon energy range, this yields an overall dynamic range of up to 7 orders of magnitude. Thus, subtle features like band tails and occupied defect states become visible. With this, deep insights into the density of occupied states (DoOS) of MHPs have been gained, including a consistent determination of the soft valence band onset;[20,23] ii) with a probing depth of 5–10 nm, near-UV CFSYS allows for the investigation of buried interfaces, whereas He-UPS is very surface sensitive and limited to a probing depth of ≈0.5–1 nm.[24]

In the present study, we investigate in detail the formation of the interface between C_{60} and a state-of-the-art mixed cation mixed halide perovskite with a precursor composition of $Cs_{0.05}(MA_{0.17}FA_{0.83})_{0.95}Pb(I_{0.83}Br_{0.17})_3$ (CsMAFA) and consider the effect of a thin LiF interlayer on the energetics at the interface.

We refine our description of the perovskite's valence band maximum (VBM)[23] to also model the superposition of the perovskite and C_{60} DoOSs for thin C_{60} layers. In this way, we can directly quantify the energy offset between the perovskite VBM and the C_{60} HOMO-edge by using a sample with an intermediate C_{60} layer thickness of 5 nm. Hence, no assumptions on the charge redistribution at the interface are required. Considering the optical band gap of C_{60} (1.92 eV) and CsMAFA (1.63 eV), we find the C_{60} LUMO-edge significantly below the perovskite conduction band minimum, which can be one reason for the limitation of the open circuit voltage.

We further show that the insertion of a LiF interlayer enhances the DoOS in the C_{60} band gap, in the first few nm of C_{60}. This should enhance non-radiative recombination, seemingly contradicting the higher V_{OC} of devices. We then reveal that the LiF interlayer also reduces the hole concentration on both sides of the interface, due to a mild dipole and probably fixed positive charge at the interface, decoupling the energy

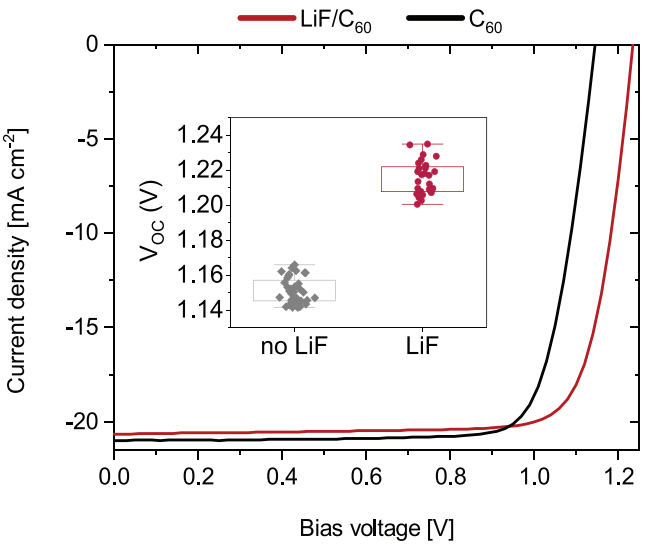

Figure 1. Effect of LiF on the current density-voltage characteristics of p-i-n perovskite solar cells with triple-cation absorber. The inset shows a boxplot of such solar cells, either with only C_{60} or with LiF/C_{60} as the electron-selective layers, as used in published high-efficiency perovskite solar cells and record perovskite-based tandem solar cells. The average increase in open-circuit voltage for the herein shown cells (n = 14) is 70 mV.

levels of CsMAFA and C_{60}. Such an effect is known, e.g., from silicon solar cells as field effect passivation,[16] and here permits to overcompensate the enhanced defect density in the first monolayers of the C_{60}, enabling a higher V_{OC}.

2. Results and Discussion

2.1. Enhancement of the Open Circuit Voltage by the LiF Interlayer

Figure 1 shows the effect of a LiF interlayer between C_{60} and the perovskite absorber on the open-circuit voltage of state-of-the-art p-i-n perovskite solar cells as used in our record perovskite/silicon tandem solar cells,[10] with the layer stack ITO/2PACz/perovskite/(LiF/)C_{60}/SnO_2/Ag. The V_{OC} substantially increases by 40–90 mV, while the fill factor and short-circuit current density remain similar. Despite LiF interlayers being used often in literature, an explanation for this large V_{OC} increase is yet missing.

To understand this gain in V_{OC}, we investigate the interface in two series of PES measurements on samples with increasing C_{60} thickness, either deposited directly on CsMAFA ("no LiF") or on CsMAFA/1 nm LiF ("LiF"). A schematic of the full "no LiF" layer stack is shown in **Figure 2**a. A reproducible mean coverage and hence contribution of C_{60} to the total density of states is confirmed by comparing the relative Pb 4f and C 1s core level peak areas upon C_{60} growth, as measured by XPS (Figures S1 and S3, Supporting Information). Furthermore, cross-section images of the layer stack from scanning electron microscopy hint to a smooth coverage of the C_{60} on the perovskite grains (Figure S4, Supporting Information). From XPS, it appears that the LiF layer remains at the interface, with no indication of dissociation (Figure S3, Supporting Information). We also find

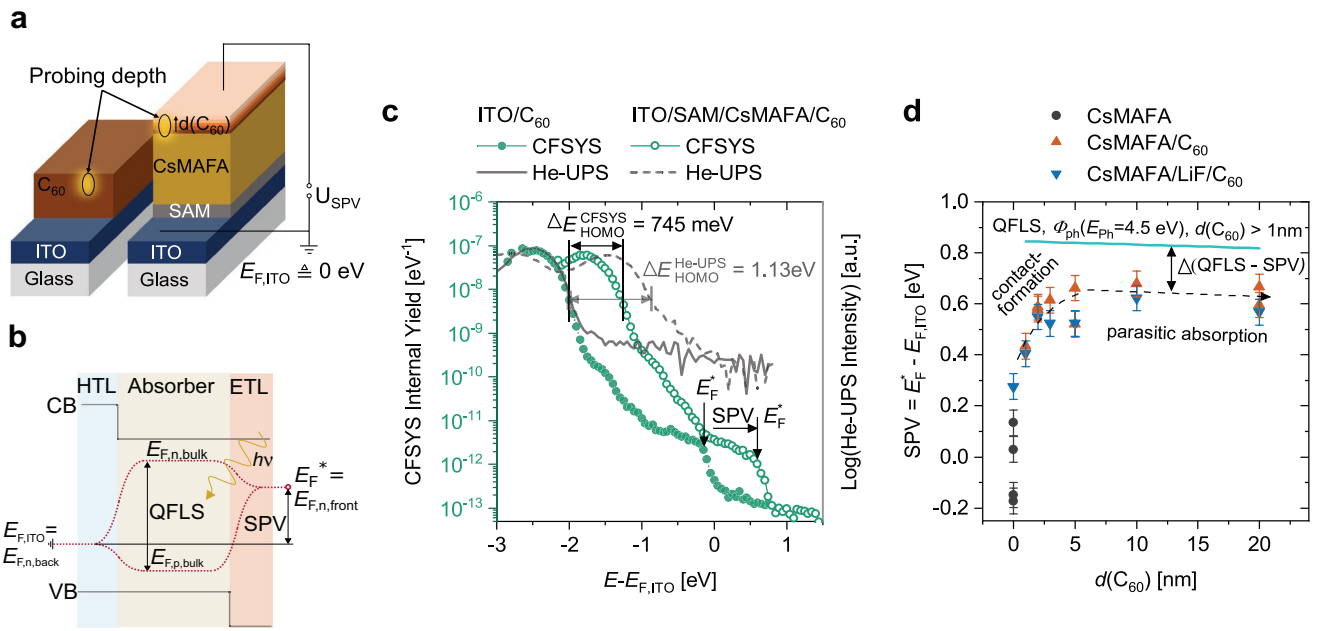

Figure 2. a) Schematic representation of the layer stacks investigated in this work: ITO/C_{60} and solar cell-like layer stack ITO/SAM/CsMAFA/C_{60}. For PES, the samples are contacted via the ITO substrate, i.e., with $E_{F,ITO}$ as reference for the binding energy scale. b) Simplified energy levels in the layer stack under near-UV illumination during CFSYS measurements. The induced quasi-Fermi level splitting (QFLS) causes a SPV between the front side ($E_{F,n,front}$) and the back side ($E_{F,n,back}$). c) CFSYS and He-UPS spectra of 50 nm C_{60} deposited directly on a conductive substrate (filled circles & full grey line) compared to 20 nm C_{60} as the top layer in a solar cell-like layer stack (open circles & dashed grey line). The C_{60} HOMO-edge, E_{HOMO}, and the surface Fermi level, E_F^*, are marked. d) SPV for varying C_{60} thickness (symbols), and the estimated maximum QFLS for the photon flux, Φ_{Ph}, from the Xe-lamp used for CFSYS at a photon energy of E_{ph} = 4.5 eV (cyan line).

carbon-fluorine bonds in the C_{60} layers, but in similar amounts for both "LiF" and "no LiF" (Figures S1 and S3, Supporting Information). These fluorine residuals most likely stem from previous evaporations in the vacuum chamber, which can lead to cross-contamination in the C_{60}. To investigate whether dissociation of the LiF and thereby doping by F^- ions is likely, we tested devices by first depositing 1 nm C_{60} and then the LiF/C_{60} contact layer stack. For these samples, we do not observe the typical increase in the open circuit voltage when inserting LiF at the interface. As the cross-contamination by fluorine can have severe effects on the interface energetics and defect formation, we want to emphasize that the C_{60} layers as they are investigated in the present study are the same as those used for state-of-the-art devices,[10,25,26] and therefore are relevant for understanding the effect of LiF on the actual device performance.

2.2. Measurement-Induced Surface Photovoltage in (Near-)UV PES Measurements

Photoelectron spectroscopy measurements always rely on the illumination of the sample under investigation to excite photoelectrons. When measuring PES on complete photoactive devices, including both a hole transporting layer (HTL) and an ETL, the sample surface is measured under at least partial operation of the solar cell. The generation of excess charge carriers by the light required for the measurement and their separation by the charge-selective layers can result in a significant voltage difference between the sample's front side and the contacted back side of the layer stack (surface photovoltage, SPV).[27,28] This SPV strongly correlates with the open circuit voltage as conventionally measured in current-voltage characteristics,[29] and is discussed in the following section.

The zero reference of the binding energy scale in PES is usually chosen as the Fermi level of a conductive sample or substrate and is ensured by a well-working electrical contact between the sample and the system, which permits excited electrons from the surface to be quickly refilled so that no charging effects occur. Here, the conductive substrate is an indium tin oxide (ITO) covered glass-substrate, defining the origin of the binding energy axis as $E_{F,ITO}$.

In Figure 2c the internal photoelectron yield of a 50 nm C_{60} thin film deposited directly on ITO (Figure 2a, left) is shown on a logarithmic scale (solid dots). The highest occupied molecular orbital (HOMO) appears at binding energies below –2 eV, above that the density of localized states in the band gap starts to decrease exponentially up to ≈0 eV, where an abrupt cut-off is visible. The C_{60} HOMO-edge position is obtained by the intercept of a linear extrapolation of the leading edge of the HOMO and the noise floor, as commonly performed in literature.[30,31] This position is indicated as a vertical line (Figure S9, Supporting Information for more details). The edge position at a binding energy of ≈0 eV marks the transition from occupied to unoccupied states, which is the definition of the Fermi level. The shape and features of the gap state density resemble previous high sensitivity UPS studies.[30,32] However, our CFSYS spectra reach 1–2 orders of magnitude higher signal-to-noise ratio, thus also enabling the direct observation of the Fermi edge. By fitting this edge position (Figure S7, Supporting Information) we can thus obtain the Fermi level on the sample's

front surface, E_F^*, under low-light operation conditions (CFSYS illumination). Without any charging or SPV effects, E_F^* would be equal to $E_{F,ITO}$.

Remarkably, when comparing this spectrum to C_{60} (20 nm) in a solar cell-like layer stack (Figure 2a), including an HTL and perovskite absorber, the whole spectrum (circles) is shifted by 745 meV. This is a "rigid" shift, i.e., both the HOMO edge and E_F^* are shifted by equal amounts. With the information depth of CFSYS being significantly below the C_{60} layer thickness, the shape of the spectrum remains the same.

The simplified energy level alignment in Figure 2b of the sample under measurement condition illustrates how this surprising finding of occupied states above $E_{F,ITO}$ can be understood. The impinging photons induce a quasi-Fermi level splitting (QFLS) and the generated excess charge carriers are selectively extracted by the HTL and ETL on both sides. The accumulation of electrons in the C_{60} then results in a net voltage difference between the electron Fermi level $E_{F,n,back}$ at the contacted back side, corresponding to $E_{F,ITO}$, and the Fermi level of the electrons at the front surface, $E_{F,n,front}$, corresponding to E_F^* obtained from fitting the measured Fermi edge. This is the definition of a surface photovoltage.[33] The actual magnitude of the SPV depends on the QFLS in the absorber as well as the properties of the interfaces with the charge-selective contacts. For non-photoactive layer stacks or photoabsorbers with high surface recombination velocities, hence no possible charge accumulation at the surface, the SPV usually is very small and can go unnoticed – especially if the Fermi edge is not resolved, as it is the case for standard He-UPS applied to semiconductors. As seen in Figure 2c, though, the SPV can be very considerable in stacks including carrier selective contacts.

In Figure 2d, the obtained SPV ($E_F^* - E_{F,ITO}$) with increasing C_{60} thickness is shown, which reaches a maximum of ≈650 meV. The estimated QFLS under the present measurement conditions (Figures S5 and S6, Supporting Information) for the photon flux at a photon energy of $E_{ph} = 4.5$ eV and a C_{60} thickness above 1 nm is also added to Figure 2d. Clearly, the UV-illumination can indeed cause such high QFLS. For the neat CsMAFA samples, E_F^* fluctuates substantially around $E_{F,ITO}$, but with the deposition of 1 nm C_{60} already a significant charge separation and thus SPV is observed, which is in agreement with thin C_{60} layers yielding considerable open circuit voltage in MHP solar cells.[34] The steep increase in SPV for low C_{60} thickness can be explained by the high surface roughness of C_{60} starting from an island growth, then coalescing into a uniform and closed layer. With further increasing C_{60} thickness, the electrons can be effectively extracted and accumulate in the C_{60}. For even thicker C_{60}, a slight decrease in SPV is found as a result of increasing parasitic absorption by the C_{60}, thus decreasing photogeneration in the perovskite.

The observed shift is not unique to the near-UV-based PES techniques: In Figure 2c the corresponding He-UPS spectra are shown. We observe a shift of 1.13 eV of the HOMO-edge relative to $E_{F,ITO}$, when comparing C_{60} directly on ITO and the solar cell-like layer stack. As the Fermi edge is hidden below the noise floor, without the additional information from CFSYS, this could have been wrongly attributed to the Fermi level being far closer to the HOMO-edge for the solar cell-like layer stack. Combining information about the energetic shifts quantified by He-UPS and NUPS/CFSYS is hence not valid as the illumination conditions vary substantially, which then affects the QFLS and SPV.

Since an SPV shifts the whole DoOS, i.e., all energetic positions relative to the substrate Fermi level, the energetic shifts can also be investigated by evaluating the core levels, observed by XPS. For thin overlayers up to ≈5 nm, depending on the light source, the core level positions from both the substrate and overlayer appear in the same spectra. The relative shifts of the core levels should in principle be in line with the energetic shifts evaluated from the CFSYS spectra. However, it has been shown that X-ray illumination can lead to significant degradation of the perovskite surface,[23,35] and by comparing CFSYS spectra of a solar cell-like layer stack with 5 nm C_{60}, we find that the contact layers gradually lose their charge selection properties upon the XPS measurement time of ≈3 h (Figure S2, Supporting Information). This induces a pronounced ambiguity – of the order of the SPV – when interpreting the core level positions in this specific case.

One further option to investigate the SPV in the layer stack with XPS and if the Fermi edge is below the detection limit of the specific system, is to compare energetic positions measured with very low illumination intensity (dark) and with a known intensity of bias light.[27,36] This requires highly efficient electron analyzers to measure such low photoelectron counting rates; an actual dark PES measurement can inherently not be reached.

Here, using CFSYS to directly observe the Fermi edge at the sample surface allows to quantify the SPV without the need for reference measurements under different illumination conditions. Note, that by referencing the C_{60} and perovskite spectra to E_F^* we implicitly assume that no voltage loss occurs at the interface/across the C_{60}.

2.3. Direct Determination of the Energetic Offsets at the CsMAFA/C_{60} Interface

After understanding the origin of the observed shift of the spectrum when measuring CFSYS on solar cell-like layer stacks, we now use the surface Fermi level obtained from model fits, E_F^*, as the new zero reference of the binding energy and can thereby evaluate the energy level alignment at the CsMAFA/C_{60} interface corrected for charging and SPV effects.

The band offsets between two adjacent semiconductors are essential to describe their energy level alignment. Conventionally, such offsets are determined by considering the band edge positions obtained by He-UPS on the free surfaces of the individual materials and assuming the Anderson rule.[37] However, at the interface, charge redistribution can occur, influenced by a different work function, but also by (interfacial) defect states and potentially Fermi level pinning, such that the bands align differently than expected by the energetic positions measured at the individual surfaces.

The photoelectrons collected in CFSYS originate from a depth of 5–10 nm with exponential damping toward the sample's depth. The accessibility of buried interfaces in PES is unique to either very low or very high kinetic energies of the photoelectrons.[24] In the most simplistic picture, for C_{60} layers

thinner than the information depth, the density of occupied states of the CsMAFA valence band is superimposed with the HOMO DoOS of the C_{60} covering the perovskite. Additionally, occupied interface defect states might contribute to the overall photoelectron yield. With an appropriate thickness of the covering layer, the energy offsets can then be directly determined from one spectrum without relying on assumptions about the charge carrier redistribution at the interface.[22,38]

To evaluate the energy offset here, we make use of our previously published band fluctuation model,[23,39] which describes the density of occupied states N_{OCC} of the two highest valence band edges of the CsMAFA perovskite in a parabolic approximation and including their exponential band tails. Each valence band edge is described with a polylogarithmic function.[23]

We account for the additional DoOS from the C_{60} HOMO by introducing a Gaussian distribution at ≈–2.5 eV with respect to E_F^*. Up to a C_{60} thickness of 5 nm the contributions of both materials to the internal yield are clearly distinguishable as shown in the exemplary fit in **Figure 3** on a (a) semi-logarithmic and (b) linear scale. Importantly, the perovskite valence band edges remain visible from below the covering C_{60} layer. For 5 nm C_{60} the interface formation can be considered as already completed and the charge carrier redistribution at the interface should be similar to the actual interface in the device with 18–23 nm C_{60}. The occupied states in the band gap are modeled by three Gaussian distributions, which are introduced to the model in order to obtain reliable fits in the energy region where the exponential band tail and the defect states overlap. However, we attach no strong physical meaning to their energetic positions as in the flat DoOS in the band gap no reliable distinct peak position can be obtained. Following the procedure established in literature,[30,31] the C_{60} HOMO-edge is obtained by a linear extrapolation of the HOMO and included in Figure 3b.

In general, the aim was to use as few as possible restrictions on the fitting model. However, to obtain a physically reasonable fit, some relative constraints on the energetic positions and amplitudes of the perovskite valence band edges were set, based on the modeling of the neat perovskite. The two parabolic band edges of the perovskite were restricted in their energetic difference and amplitude ratio between each other. However, their energetic position with respect to E_F^* was used as a free fitting parameter (see experimental details, Supporting Information).

From the combined model fit we can then directly determine the offset between the perovskite valence band maximum and the C_{60} HOMO-edge to ΔE_V = 0.55 eV. For C_{60} as the electron transporting layer, the energy offset of the CsMAFA conduction band minimum and the C_{60} LUMO-edge ΔE_C is of special importance. Considering the optical band gap energies of the respective materials this offset can be determined as ΔE_C = 0.26 eV. Here, the optical band gap of C_{60} is evaluated from a combination of spectroscopic ellipsometry, reflection, and transmission measurements to a value of 1.92 eV (Figures S10 and S11, Supporting Information). With the band gap energy of the investigated perovskite composition being 1.63 eV, a type 2 heterojunction with staggered gap is found. The "downwards" offset between the perovskite conduction band edge and C_{60} LUMO-edge is in line with the limitation of the open

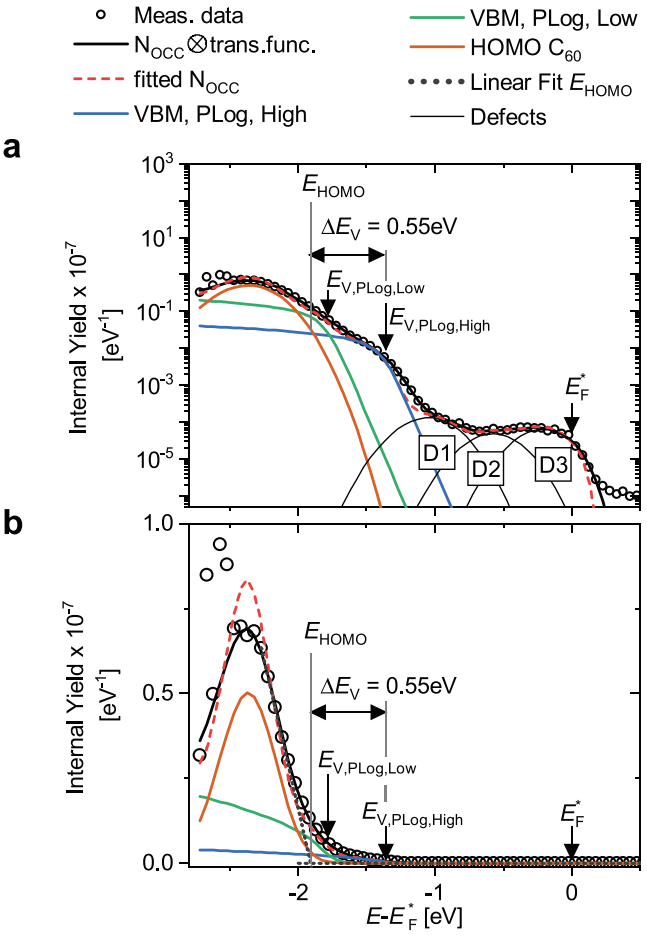

Figure 3. Model fit of the density of occupied states, N_{OCC}, to a CFSYS spectrum, obtained for a 5 nm C_{60} thin film on ITO/MeO-2PACz/CsMAFA: a) semi-logarithmic, and b) linear scale. The model consists of two parabolic band edges with an exponential band tail, representing the perovskite valence band edges (green, blue), a Gaussian distribution, representing the C_{60} HOMO (orange), and three Gaussian distributions, accounting for the occupied states in the band gap (grey). The modeled N_{OCC} is convolved with the system transfer function. The energy offset between the perovskite VBM and the C_{60} HOMO-edge, $\Delta E_V = E_{HOMO} - E_{V,PLog,high}$, is directly determined from the fit parameters.

circuit voltage of the actual device:[12] Once the photogenerated electrons are transferred from the CsMAFA to the C_{60}, they thermalize to the lower-lying LUMO and thereby lose the band offset energy ΔE_C. Note, that the energy offset as obtained here slightly exceeds the reported difference between QFLS with and without C_{60}, which is in the order of 50–100 meV.[8] As soon as the LUMO-edge is located below the quasi-Fermi level of the electrons in the perovskite, it starts to limit the overall V_{OC} as seen for illumination-dependent V_{OC} measurements and different perovskite/HTL interfaces.[40]

The reported energy offsets in literature for similar (perovskite/C_{60}) interfaces vary substantially,[12,27,41,42] which is due to two main reasons: i) the valence band offset might be underestimated because of an unrecognized SPV in p-i-n solar cell-like layer stacks, which then shifts the HOMO-edge position closer to the back-contacted reference Fermi level $E_{F,ITO}$. If the

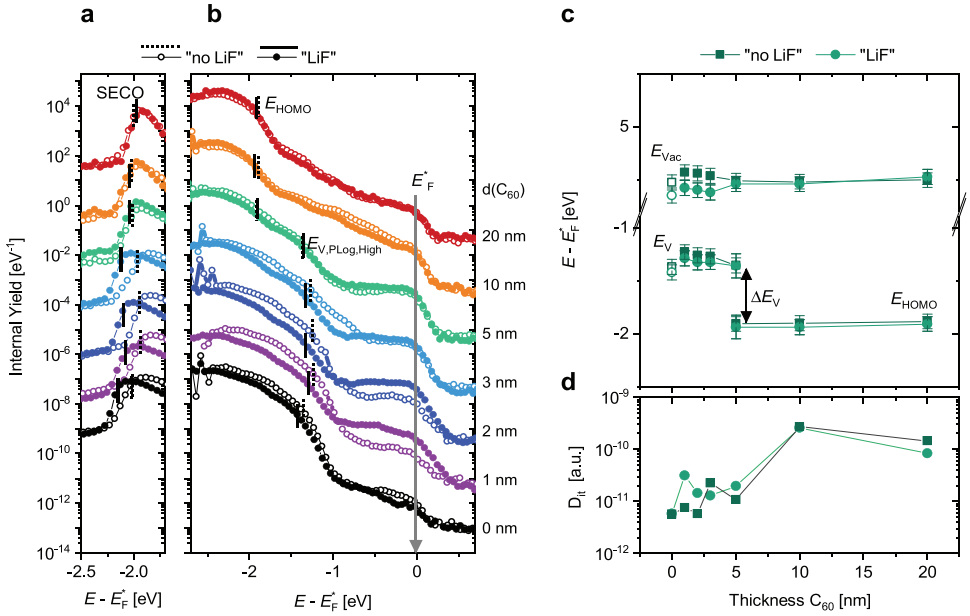

Figure 4. Comparison of spectra and energetic positions for varying C_{60} thickness on glass/ITO/MeO-2PACz/(LiF)/CsMAFA with LiF interlayer ("LiF") and without ("no LiF"): a) Secondary electron cut-off (SECO), measured by NUPS (6.5 eV excitation energy). b) CFSYS spectra with the perovskite valence band maximum ($E_{V,PLog,High}$), and the C_{60} HOMO-edge (E_{HOMO}) indicated as vertical lines. c) Energetic positions with respect to the surface Fermi level, E_F^* obtained by the combined modeling of the CFSYS and NUPS spectra.

Fermi-edge is not directly visible in the spectra and if further no varying illumination conditions, i.e., additional bias light, are considered, it is difficult to judge the reliability of the reported values; ii) the assumption of largely different band gaps of C_{60} directly affects the determination of the conduction band offset. The electrical band gap of C_{60} is often determined by combined inverse photoelectron spectroscopy and PES to be ≈2.3 eV,[41,43] but also lower values of ≈1.7 eV are reported,[8] again potentially suffering from SPV effects in the PES measurements. Note, that herein we used the optical band gap and can hence exclude SPV effects. However, it is known, that the optical band gap energy is slightly lower than the electrical one, due to a high exciton binding energy.[43,44]

To summarize, we quantify the SPV effects and additionally do not rely on assumed charge transfer processes at the interface and thereby directly determine the energy offset between the CsMAFA valence band maximum and C_{60} HOMO-edge to 0.55 eV. This ensures efficient hole blocking. Using the optical band gaps, we calculate a large "downwards" conduction band offset of 0.26 eV. This allows the electrons to pass the interface, but contributes to the limitation of the open circuit voltage by the C_{60} interface, as is reported in literature.[11,40]

2.4. Influence of a LiF Interlayer at the CsMAFA/LiF/C_{60} Interface

We investigate the influence of LiF on the interface between CsMAFA and C_{60} by monitoring the work function, perovskite valence band maximum, and C_{60} HOMO-edge for different thicknesses of C_{60}. To that end, C_{60} was evaporated with a thickness of 1 to 20 nm on the CsMAFA in two sample series, either directly on the perovskite ("no LiF") or with LiF interlayer ("LiF"). The spectra have then been fitted with the combined model as it was introduced above. In **Figure 4** the internal yield of (a) the secondary electron cut-off (SECO), measured by NUPS, and (b) the density of states in the valence band region up to the Fermi edge, measured by CFSYS, are shown for the full thickness variation from 0 nm (bare perovskite) to 20 nm C_{60}. The obtained energetic positions (SECO, $E_{V,PLog,High}$ and E_{HOMO}) are indicated in the spectra with dashed lines ("no LiF") and solid lines ("LiF").

Qualitatively, both with and without the LiF interlayer, the shape of the DoOS in the valence band and HOMO region is similar and the measured internal yield evolves gradually from bare perovskite toward the density of states of thick C_{60} films. Note again the probing depth of 5–10 nm of the NUPS and CFSYS. For thin C_{60} layers up to 3 nm, the valence band maximum as well as the SECO of the LiF-containing layer stacks are found to shift toward lower energies with respect to the surface Fermi level E_F^*.

The shape of the spectra evolves in three stages: i) For a layer thickness up to 2 nm the shape of the spectrum appears mostly perovskite-like and only the density of defect states in the energy region between 0 and –1 eV slightly changes. The appearance of the C_{60} HOMO-peak at ≈–2.5 eV is barely visible for these thin C_{60} layers; ii) For an intermediate thickness of 3 to 5 nm the square-root behavior of the perovskite valence band edges is still visible, but simultaneously the DoOS of the C_{60} HOMO with its center at ≈–2.5 eV increases; and iii) For 10 nm and 20 nm C_{60} the parabolic perovskite band edges are not contributing anymore to the overall internal yield and an exponentially decaying density of states is apparent between –1.8 eV and 0 eV. The spectrum then resembles the thick 50 nm film on ITO (see also Figure 2c) as mostly C_{60} is probed, without additional contribution from the interface-near defect states.

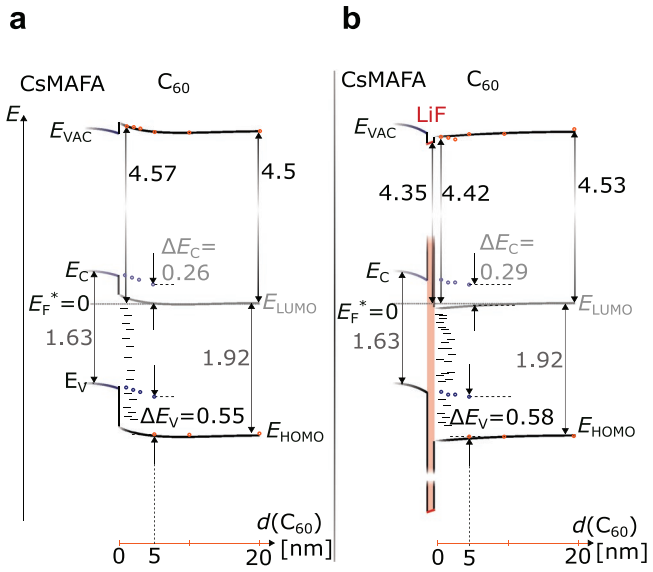

Figure 5. Energy level alignment at the CsMAFA(/1 nm LiF)/C_{60} interface, obtained by detailed analysis of NUPS and CFSYS spectra for a) "no LiF" and b) "LiF". All energetic positions are given relative to the surface Fermi level, E_F^*, and in units of eV. The C_{60} HOMO-edge, the perovskite VBM and the work function are indicated as dots (blue for perovskite and orange for C_{60}). The optical band gaps of CsMAFA and C_{60} (values in grey) are used for an estimation of the perovskite conduction band edge and the C_{60} LUMO-edge.

The energy positions for both series are summarized in Figure 4c. The perovskite valence band edges can be modeled as in our previous publication[23] up to a thickness of 5 nm C_{60}; from 5 nm onwards the HOMO-edge E_{HOMO} of C_{60} can be determined. The combined energy level alignment is also depicted in **Figure 5** in the next section.

The valence band maximum of the perovskite is found to slightly shift away from E_F^* for increasing C_{60} thickness. For the very thinnest C_{60} layers deposited on LiF interlayers, the Fermi level is found ≈50 meV closer to the conduction band minimum as compared to "no LiF". This points toward a higher electron concentration close to the interface in the perovskite, probably caused by a positive fixed charge. Historically, such an effect of passivation by reduced minority charge carrier concentration at the surface/interface is well-known, e.g., from silicon solar cells,[16] where it was termed field effect passivation. Recently, it has also been reported for perovskite solar cells.[45] With our CFSYS data, we can demonstrate that a similar mechanism lies behind the passivating effect of LiF at the perovskite/C_{60} interface.

Furthermore, we observe a decrease of 130 meV in the work function for 1 nm LiF on the perovskite without any C_{60}, in comparison to the bare perovskite (Figure 4c, open symbols). For thin layers of C_{60} up to 3 nm, this reduction in work function by ≈150 meV persists. Note, that the LiF samples had to be transferred through an inert atmosphere, which might have an influence on the wok function as it is very sensitive to even minor changes of the surface chemistry.

The HOMO-edge of C_{60} for 5 nm or thicker C_{60} remains at ≈–1.9 eV, yielding ionization energies of 6.4 eV for both series "no LiF" and "LiF". If the material itself does not change (i.e., no hybridization occurring[46]), the ionization energy should not depend on the C_{60} thickness, and hence the HOMO-edge can be expected to follow the trend of the work function for layers thinner than 5 nm, where it cannot be directly evaluated.

With the discussed HOMO-edge of the C_{60} and valence band maximum of the perovskite, we find ΔE_V = 0.58 eV and ΔE_C = 0.29 eV for the "LiF" samples, both being slightly higher as compared to "no LiF", evaluated in the previous section, and still in the error margin. A change in the energetic offsets implies either a change in the C_{60} properties close to the interface or the existence of an interfacial dipole layer.

To evaluate the defect density, the shape of the DoOS in the band gap, i.e., above the exponential band tail, in Figure 4b is considered.

The CFSYS spectra for samples with a C_{60} thickness up to 5 nm show a rather flat distribution of the density of occupied gap states between –1 eV and 0 eV. For the bare perovskite and the additional deposition of 1 nm LiF, the density of gap states stays at a similarly low level. Only between the Fermi edge and –0.5 eV it is slightly decreased for "LiF". This decrease is however barely visible and within the same range as typical variations of the defect density in the bare perovskite.

For a C_{60} layer thickness between 1 nm and 2 nm on top of the CsMAFA, the defect density abruptly increases by roughly one order of magnitude for the "LiF" series, as compared to "no LiF". In addition to the discussed downwards conduction band offset, such a defect density, present even without the LiF, can contribute to the observed V_{OC} limitation in cells. However, we note that defect states in the perovskite are also generated by the UV light of the measurement[23,47] and might already be at a level where they also contribute to the CFSYS signal in the relevant energy range.

The deviation between both series is less pronounced but still existent for 3 to 5 nm C_{60} thickness. For 3 nm C_{60} without LiF, an exceptional shape of the gap state density with a distinct shoulder at ≈–1 eV with respect to E_F^* is observed. A similar peak shape appeared for a neat perovskite sample after prolonged vacuum storage.[23] Even though no prolonged vacuum storage occurred for the herein investigated samples, this clear defect peak is probably indicating a degraded perovskite surface in that case, even before the deposition of the thin C_{60} layer. Considering the DoOS is closer to the Fermi level, the defect density is still slightly enhanced (see Figure S12, Supporting Information).

For a higher C_{60} thickness beyond 5 nm, the shape of the gap state density changes and is found to decay exponentially into the band gap for both "LiF" and "no LiF" samples. The highest defect density is obtained for a film thickness of 10 nm for both series, where states close to the CsMAFA/LiF/C_{60} interface still contribute, and then again decreases for thicker films with 20 nm C_{60}.

It has been reported for very similar perovskite compositions that the main beneficial effect of the LiF interlayer is the suppression of non-radiative interface recombination of the photo-generated charge carriers, thus enhanced interface passivation.[7,48,49] For some buffer layers, such as choline chloride, also chemical passivation of defects in the perovskites was suggested,[50] and additionally, fluorine ions have been reported to passivate perovskites by, e.g., the substitution of halide

vacancies or forming chemical bonds to the organic cation and halide anions, which prevents them from moving in the perovskite crystal and thus also enhance both the passivation and device stability.[49,51] A chemical passivation of occupied defect states in the perovskite close to the interface can however not be supported with the herein presented results. In this study, it was found that the defect density in the first monolayers of the C_{60} is enhanced when inserting a thin LiF interlayer. Warby et al. concluded from a photoluminescence analysis that the mechanism behind the V_{OC} limitation by the C_{60} ETL can be attributed to defect states in the C_{60} close to the interface.[12] A strong contribution by interface-near defect states without LiF can however not be confirmed by our measurements. As the enhanced defect density with LiF clearly starts to appear only once C_{60} is deposited on the layer stack, we conclude that they must be located in the very first nm of C_{60}, i.e., not in the perovskite, which in general fits the analysis of Warby et al.[12]

To sum up, the insertion of a thin 1 nm LiF interlayer at the CsMAFA/LiF/C_{60} interface increases the defect density in the first monolayers of C_{60} up to 5 nm. An enhanced defect density should however be detrimental to the device performance, especially the open circuit voltage, while the opposite effect is observed for devices. To understand this phenomenon the overall picture of the energy level alignment needs to be considered and will be discussed in the next section.

2.5. Energy Level Alignment of the CsMAFA/LiF/C_{60} Interface

Combining the evaluated energetic positions above, the formation of the CsMAFA/C_{60} interface and the energy level alignment with the insertion of an ultra-thin LiF interlayer will be discussed here.

In Figure 5 the energy level alignment for varying C_{60} thickness is shown a) without a LiF interlayer and b) with a 1 nm LiF interlayer. The energetic positions (same as in Figure 4c) are indicated as dots in the diagram (blue for perovskite and orange for C_{60}) and are obtained by the combined fitting model of the perovskite VBM and the C_{60} HOMO-edge. It is important to note, that each C_{60} thickness can lead to a different charge balance at the interface. Hence, the drawing should not be considered as a depth profile, but as several individual cases (different C_{60} thicknesses) condensed into one graph. For example, for different C_{60} thicknesses, we observe a varying energetic distance between the perovskite valence band edge and the Fermi level, indicating already a different charge redistribution for different C_{60} thicknesses. These spectra of the thinnest layers are of high importance as they also reveal the energetics of the perovskite at the actual interface below the C_{60}. From measuring C_{60} thicker than the probing depth, no detailed conclusions about the interface formation can be drawn, since only the surface is probed. This is a general problem of energy level alignments obtained by PES and their visual representation as shown here (and commonly in literature). Furthermore, it highlights the importance of the direct band offset determination.

For thin C_{60} layers, no HOMO-edge could be obtained by the modeling of the spectra. As the work function is a surface property and thus a property of the C_{60}, we can calculate the energetic position of E_{HOMO} also for the thinnest films (1–3 nm C_{60}) by assuming constant ionization energy for different C_{60} film thicknesses.[52,53]

For "no LiF", the trend of the work function of the C_{60} matches well the trend of the perovskite valence band edge. Hence, the charge balance across the interface is consistent, and constant band offsets are present at the interface for different C_{60} thicknesses. In contrast, for the "LiF" samples, the work function decreases for decreasing C_{60} thickness, indicating an electron accumulation and potentially a slight downwards band bending in the C_{60} toward its interface with LiF. At the same time, the VBM of the perovskite shows the opposite trend, leading to an increase of ΔE_V for thinner C_{60} layers. This could hint to a significant positive fixed charge in the interlayer, leading to electrostatic screening and decoupling the C_{60} from the perovskite.[54] In the end, based on our modeling, the Fermi level is found closer to the conduction band minimum of the perovskite as compared to the "no LiF" case, implying a higher electron and lower hole concentration. Further, such change in the charge carrier concentration can also stem from chemical changes at the interface. We do not find any indication for this in the core level spectra, but we want to note that such doping effects can also lead to chemical changes which are below the resolution of our XPS measurements.

We have discussed how the charge transfer across this interface strongly changes upon the deposition of the electron accepting C_{60}, leading to strong SPV effects. Thus, the energetic position of the Fermi level in the band gap changes upon deposition of a C_{60} contact layer. Consequently, for the sketch of the band line-up in Figure 5 only the energetic positions from samples with at least 1 nm C_{60} are considered. We sketch a slight downwards band bending in the perovskite, based on the assumption of a (more) intrinsic behavior in the perovskite bulk than at the surface.[36] Since the distance of $E_{V,PLog,High}$ to the surface Fermi level E_F^* is found to be slightly larger for "LiF", also the band bending is stronger here, assuming similar bulk properties of the perovskite.

Besides a fixed charge in the interlayer, a potential dissociation of LiF and thereby interfacial doping of C_{60} by fluorine ions might also lead to an increased electron and reduced hole concentration at the interface. Such doping effects have been observed when depositing Al on a C_{60}/LiF layer stack.[55,56] As mentioned above, due to cross-contamination, we find fluorine in similar amounts for "LiF" and "no LiF" in device-relevant layers. Therefore, the presence of F^- ions is probably not the main driver of the observed voltage enhancement.

Overall, based on the modeling of the CFSYS spectra, we suggest that the fixed charge and/or dipole induced by the LiF leads to an increased electron density at the interface for "LiF" compared to a depleted interface for "no LiF" samples. This enables a better electron transfer due to higher conductivity across the interface. Furthermore, with a decoupling of the CsMAFA and the C_{60}, a slightly higher valence band offset, and hence a more efficient hole blocking can be obtained. Consequently, the hole concentration will be reduced in the vicinity of the interface. This might be the key mechanism to the enhanced QFLS and cell V_{OC}s with LiF interlayers: it implies a more asymmetric charge carrier concentration, ultimately leading to less non-radiative recombination across the interface,

despite enhanced defect densities in the first monolayers of the C_{60}.

3. Conclusion

Using near-UV constant final state yield photoelectron spectroscopy (CFSYS), we studied the electronic interface formation and energy level alignment of C_{60} as an electron transporting material with a mixed cation mixed halide perovskite (CsMAFA, $Cs_{0.05}(MA_{0.17}FA_{0.83})_{0.95}Pb(I_{0.83}Br_{0.17})_3$). Furthermore, the influence of a 1 nm LiF interlayer between the perovskite and the C_{60} on the energy level alignment at this interface was investigated, since this is one of the most used interface passivation strategies for p-i-n perovskite solar cells.[7,10]

By directly observing the Fermi edge in the CSFYS spectra, we can account for measurement-induced surface photovoltage effects in the photoactive layer stacks and directly reference the energetic positions to the actual surface Fermi level. With an unusually high probing depth of 5–10 nm, which is intrinsic to the near-UV CFSYS, we were able to measure the superimposed density of occupied states of thin C_{60} layers and the underlying perovskite. A band fluctuation model for the two highest perovskite valence band edges[23] was further expanded to include the C_{60} HOMO level. Based on this model and using a sample with 5 nm C_{60}, the band offset between the perovskite valence band maximum and the C_{60} HOMO-edge could be directly evaluated and modeled in one spectrum, it was found to be 0.55 eV. With the band gap of the investigated perovskite composition of 1.63 eV and an optical band gap of 1.92 eV for C_{60}, the energy offset between the perovskite conduction band minimum and the C_{60} LUMO is thus determined to be 0.26 eV. This large conduction band offset as well as the non-vanishing density of gap states in the C_{60} can cause the V_{OC} limitation by the C_{60} electron transporting layer as reported in literature.

In literature, a reduced non-radiative charge carrier recombination at the perovskite/LiF/C_{60} interface has been demonstrated.[7] Surprisingly, we find here that a LiF interlayer at the perovskite/C_{60} interface induces an enhanced defect density in the first monolayers of C_{60}. This could be expected to increase trap-assisted recombination, and thus lower V_{OC} in a cell. However, considering our CFSYS data, we surmise that the detrimental effect of the defects might be overcompensated by a reduced hole density in the vicinity of the perovskite/C_{60} interface. This can be caused by a small dipole and probably positive fixed charges. Linking to established solar cell technologies, the passivation mechanism of LiF might therefore be called a field effect passivation.

Supporting Information

Supporting Information is available from the Wiley Online Library or from the author.

Acknowledgements

The authors acknowledge funding by the Federal Ministry of Education and Research (BMBF) under the Grant 03SF0631 (PEROWIN), the Helmholtz Association within the HySPRINT Innovation lab project, and the HyPerCells joint Graduate School. Furthermore, this work was supported in part by the German Federal Ministry for Economic Affairs and Climate Action under Grants 03EE1017B (Project P3T) and 03EE1086C (PrEsto), and the joint agreement between the DAAD (German Academic Exchange Service) and FONDECYT (National Fund for Scientific, Technological Development and Technological Innovation) under the agreements 57508544 DAAD and 423-2019-FONDECYT. Further support had been provided by the PUCP vice chancellorship for research (VRI, Project No. CAP-2019-3-0041/702). The authors thank Thomas Lußky for technical support and Bor Li for part of the sample preparation. Danbi Yoo is acknowledged for assistance with optical spectroscopy. Additionally, the authors thank Tilmann Neubert for the fruitful discussion about the XPS core level modeling. I.L. thanks the AiF project (ZIM-KK5085302DF0) for financial support.

Open access funding enabled and organized by Projekt DEAL.

Conflict of Interest

The authors declare no conflict of interest.

Data Availability Statement

The data that support the findings of this study are available from the corresponding author upon reasonable request.

Keywords

C_{60}, defects, energy level alignment, halide perovskites, passivation interlayers, photoemission spectroscopy, solar cells

Received: March 30, 2022
Revised: May 17, 2022
Published online:

[1] D. P. McMeekin, G. Sadoughi, W. Rehman, G. E. Eperon, M. Saliba, M. T. Hörantner, A. Haghighirad, N. Sakai, L. Korte, B. Rech, M. B. Johnston, L. M. Herz, H. J. Snaith, *Science* **2016**, *351*, 151.

[2] M. A. Green, E. D. Dunlop, J. Hohl-Ebinger, M. Yoshita, N. Kopidakis, A. W. Y. Ho-Baillie, *Prog Photovolt Res Appl* **2020**, *28*, 3.

[3] "National Renewable Energy Laboratory, *Best Research-Cell Efficiency Chart," can be found under* www.nrel.gov/pv/cell-efficiency.html, **2021**.

[4] K. Jäger, L. Korte, B. Rech, S. Albrecht, *Opt. Express* **2017**, *25*, A473.

[5] M. Jošt, E. Köhnen, A. B. Morales-Vilches, B. Lipovšek, K. Jäger, B. Macco, A. Al-Ashouri, J. Krč, L. Korte, B. Rech, R. Schlatmann, M. Topič, B. Stannowski, S. Albrecht, *Energy and Environmental Science* **2018**, *11*, 3511.

[6] P. Schulz, E. Edri, S. Kirmayer, G. Hodes, D. Cahen, A. Kahn, *Energy Environ. Sci.* **2014**, *7*, 1377.

[7] M. Stolterfoht, C. M. Wolff, J. A. Márquez, S. Zhang, C. J. Hages, D. Rothhardt, S. Albrecht, P. L. Burn, P. Meredith, T. Unold, D. Neher, *Nat. Energy* **2018**, *3*, 847.

[8] C. M. Wolff, P. Caprioglio, M. Stolterfoht, D. Neher, *Adv. Mater.* **2019**, *31*, 1902762.

[9] A. Rajagopal, R. J. Stoddard, S. B. Jo, H. W. Hillhouse, A. K.-Y. Jen, *Nano Lett.* **2018**, *18*, 3985.

[10] A. Al-Ashouri, E. Köhnen, B. Li, A. Magomedov, H. Hempel, P. Caprioglio, J. A. Márquez, A. B. M. Vilches, E. Kasparavicius,

J. A. Smith, N. Phung, D. Menzel, M. Grischek, L. Kegelmann, D. Skroblin, C. Gollwitzer, T. Malinauskas, M. Jošt, G. Matič, B. Rech, R. Schlatmann, M. Topič, L. Korte, A. Abate, B. Stannowski, D. Neher, M. Stolterfoht, T. Unold, V. Getautis, S. Albrecht, *Science* **2020**, *370*, 1300.

[11] M. Stolterfoht, P. Caprioglio, C. M. Wolff, J. A. Márquez, J. Nordmann, S. Zhang, D. Rothhardt, U. Hörmann, Y. Amir, A. Redinger, L. Kegelmann, F. Zu, S. Albrecht, N. Koch, T. Kirchartz, M. Saliba, T. Unold, D. Neher, *Energy Environ. Sci.* **2019**, *12*, 2778.

[12] J. Warby, F. Zu, S. Zeiske, E. Gutierrez-Partida, L. Frohloff, S. Kahmann, K. Frohna, E. Mosconi, E. Radicchi, F. Lang, S. Shah, F. Peña-Camargo, H. Hempel, T. Unold, N. Koch, A. Armin, F. De Angelis, S. D. Stranks, D. Neher, M. Stolterfoht, *Adv. Energy Mater.* **2022**, *12*, 2103567.

[13] M. You, H. Wang, F. Cao, C. Zhang, T. Zhang, L. Kong, L. Wang, D. Zhao, J. Zhang, X. Yang, *ACS Appl. Mater. Interfaces* **2020**, *12*, 43018.

[14] F. Peña-Camargo, P. Caprioglio, F. Zu, E. Gutierrez-Partida, C. M. Wolff, K. Brinkmann, S. Albrecht, T. Riedl, N. Koch, D. Neher, M. Stolterfoht, *ACS Energy Lett.* **2020**, *5*, 2728.

[15] R. Quintero-Bermudez, J. Kirman, D. Ma, E. H. Sargent, R. Quintero-Torres, *J. Phys. Chem. Lett.* **2020**, *11*, 4213.

[16] R. S. Bonilla, C. Reichel, M. Hermle, P. R. Wilshaw, *SSP* **2013**, *205–206*, 346.

[17] S. Béchu, M. Ralaiarisoa, A. Etcheberry, P. Schulz, *Adv. Energy Mater.* **2020**, *10*, 1904007.

[18] S. Tao, I. Schmidt, G. Brocks, J. Jiang, I. Tranca, K. Meerholz, S. Olthof, *Nat. Commun.* **2019**, *10*, 2560.

[19] F. Zhang, S. H. Silver, N. K. Noel, F. Ullrich, B. P. Rand, A. Kahn, *Adv. Energy Mater.* **2020**, 1903252.

[20] I. Levine, K. Shimizu, A. Lomuscio, M. Kulbak, C. Rehermann, A. Zohar, M. Abdi-Jalebi, B. Zhao, S. Siebentritt, F. Zu, N. Koch, A. Kahn, G. Hodes, R. H. Friend, H. Ishii, D. Cahen, *J. Phys. Chem. C* **2021**, *125*, 5217.

[21] J.-P. Yang, M.-F. Yang, G. Tang, S. Kera, *J. Phys.: Condens. Matter* **2021**, *33*, 475001.

[22] M. Sebastiani, L. Di Gaspare, G. Capellini, C. Bittencourt, F. Evangelisti, *Phys. Rev. Lett.* **1995**, *75*, 3352.

[23] D. Menzel, A. Tejada, A. Al-Ashouri, I. Levine, J. A. Guerra, B. Rech, S. Albrecht, L. Korte, *ACS Appl. Mater. Interfaces* **2021**, *13*, 43540.

[24] M. P. Seah, W. A. Dench, *Surf. Interface Anal.* **1979**, *1*, 2.

[25] A. Al-Ashouri, A. Magomedov, M. Roß, M. Jošt, M. Talaikis, G. Chistiakova, T. Bertram, J. A. Márquez, E. Köhnen, E. Kasparavičius, S. Levcenco, L. Gil-Escrig, C. J. Hages, R. Schlatmann, B. Rech, T. Malinauskas, T. Unold, C. A. Kaufmann, L. Korte, G. Niaura, V. Getautis, S. Albrecht, *Energy Environ. Sci.* **2019**, *5*, 1035.

[26] P. Tockhorn, J. Sutter, R. Colom, L. Kegelmann, A. Al-Ashouri, M. Roß, K. Jäger, T. Unold, S. Burger, S. Albrecht, C. Becker, *ACS Photonics* **2020**, *7*, 2589.

[27] T. Hellmann, C. Das, T. Abzieher, J. A. Schwenzer, M. Wussler, R. Dachauer, U. W. Paetzold, W. Jaegermann, T. Mayer, *Adv. Energy Mater.* **2020**, *10*, 2002129.

[28] J. Frisch, M. Schubert, E. Preis, J. P. Rabe, D. Neher, U. Scherf, N. Koch, *J. Mater. Chem.* **2012**, *22*, 4418.

[29] N. Kedem, M. Kulbak, T. M. Brenner, G. Hodes, D. Cahen, *Phys. Chem. Chem. Phys.* **2017**, *19*, 5753.

[30] F. Bussolotti, J. Yang, M. Hiramoto, T. Kaji, S. Kera, N. Ueno, *Phys. Rev. B* **2015**, *92*, 115102.

[31] Y. Nakayama, T. L. Nguyen, Y. Ozawa, S. Machida, T. Sato, H. Tokairin, Y. Noguchi, H. Ishii, *Adv. Energy Mater.* **2014**, *4*, 1301354.

[32] S. Machida, Y. Ozawa, J. Takahashi, H. Tokairin, Y. Nakayama, H. Ishii, *Appl. Phys. Express* **2013**, *6*, 025801.

[33] D. K. Schroder, *Meas. Sci. Technol.* **2001**, *12*, R16.

[34] D. Liu, Q. Wang, C. J. Traverse, C. Yang, M. Young, P. S. Kuttipillai, S. Y. Lunt, T. W. Hamann, R. R. Lunt, *ACS Nano* **2018**, *12*, 876.

[35] W.-C. Lin, W.-C. Lo, J.-X. Li, Y.-K. Wang, J.-F. Tang, Z.-Y. Fong, *npj Mater. Degrad.* **2021**, *5*, 13.

[36] F.-S. Zu, P. Amsalem, I. Salzmann, R.-B. Wang, M. Ralaiarisoa, S. Kowarik, S. Duhm, N. Koch, *Adv. Opt. Mater.* **2017**, *5*, 1700139.

[37] R. L. Anderson, *IBM J. Res. Dev.* **1960**, *4*, 283.

[38] L. Korte, R. Rößler, C. Pettenkofer, *J. Appl. Phys.* **2014**, *115*, 203715.

[39] J. A. Guerra, A. Tejada, J. A. Töfflinger, R. Grieseler, L. Korte, *J. Phys. D: Appl. Phys.* **2019**, *52*, 105303.

[40] P. Caprioglio, M. Stolterfoht, C. M. Wolff, T. Unold, B. Rech, S. Albrecht, D. Neher, *Adv. Energy Mater.* **2019**, *9*, 1901631.

[41] P. Schulz, L. L. Whittaker-Brooks, B. A. MacLeod, D. C. Olson, Y.-L. Loo, A. Kahn, *Adv. Mater. Interfaces* **2015**, *2*, 1400532.

[42] C. Wang, X. Liu, C. Wang, Z. Xiao, C. Bi, Y. Shao, J. Huang, Y. Gao, *J. Vac. Sci. Technol., B: Nanotechnol. Microelectron.: Mater., Process., Meas., Phenom.* **2015**, *33*, 032401.

[43] R. W. Lof, M. A. van Veenendaal, B. Koopmans, H. T. Jonkman, G. A. Sawatzky, *Phys. Rev. Lett.* **1992**, *68*, 3924.

[44] B. Stadtmüller, S. Emmerich, D. Jungkenn, N. Haag, M. Rollinger, S. Eich, M. Maniraj, M. Aeschlimann, M. Cinchetti, S. Mathias, *Nat. Commun.* **2019**, *10*, 1470.

[45] F. Wang, Y. Zhang, M. Yang, D. Han, L. Yang, L. Fan, Y. Sui, Y. Sun, X. Liu, X. Meng, J. Yang, *Adv. Funct. Mater.* **2021**, *31*, 2008052.

[46] B. W. Hoogenboom, R. Hesper, L. H. Tjeng, G. A. Sawatzky, *Phys. Rev. B* **1998**, *57*, 11939.

[47] A. Farooq, M. R. Khan, T. Abzieher, A. Voigt, D. C. Lupascu, U. Lemmer, B. S. Richards, U. W. Paetzold, *ACS Appl. Energy Mater.* **2021**, *4*, 3083.

[48] Z. Li, K. Cao, J. Li, X. Du, Y. Tang, B. Yu, *Org. Electron.* **2020**, *81*, 105675.

[49] A. J. Yun, J. Kim, B. Gil, H. Woo, K. Park, J. Cho, B. Park, *ACS Appl. Mater. Interfaces* **2020**, *12*, 50418.

[50] X. Zheng, B. Chen, J. Dai, Y. Fang, Y. Bai, Y. Lin, H. Wei, X. C. Zeng, J. Huang, *Nat. Energy* **2017**, *2*, 17102.

[51] N. Li, S. Tao, Y. Chen, X. Niu, C. K. Onwudinanti, C. Hu, Z. Qiu, Z. Xu, G. Zheng, L. Wang, Y. Zhang, L. Li, H. Liu, Y. Lun, J. Hong, X. Wang, Y. Liu, H. Xie, Y. Gao, Y. Bai, S. Yang, G. Brocks, Q. Chen, H. Zhou, *Nat. Energy* **2019**, *4*, 408.

[52] X. Liu, S. Yi, C. Wang, C. Wang, Y. Gao, *J. Appl. Phys.* **2014**, *115*, 163708.

[53] F. J. Zhang, A. Vollmer, J. Zhang, Z. Xu, J. P. Rabe, N. Koch, *Org. Electron.* **2007**, *8*, 606.

[54] N. B. Kotadiya, H. Lu, A. Mondal, Y. Ie, D. Andrienko, P. W. M. Blom, G.-J. A. H. Wetzelaer, *Nature Mater* **2018**, *17*, 329.

[55] E. D. Głowacki, K. L. Marshall, C. W. Tang, N. S. Sariciftci, *Appl. Phys. Lett.* **2011**, *99*, 043305.

[56] Y. Yuan, D. Grozea, S. Han, Z. H. Lu, *Appl. Phys. Lett.* **2004**, *85*, 4959.